IMPACT OF AN UNDERWATER EXPLOSION ON CRITICAL INFRASTRUCTURE: AN EXPERIMENTAL SMALL-SCALE INVESTIGATION

ORIANE DEGLETAGNE[1], SOPHIE TRÉLAT[1] & MICHEL-OLIVIER STURTZER[2]
[1]DEND, French Institute for Protection and Nuclear Security,
Department of Explosion and Weapons Effects, Fontenay-aux-Roses, France
[2]ISL, French German Research Institute of Saint-Louis,
Department of Explosive Protection, Saint-Louis, France

ABSTRACT

This study investigates the effects of underwater explosions on critical infrastructures, with a focus on structures commonly found in the nuclear sector. The research addresses the potential consequences of detonation (accidental or deliberate) on industrial pools and other containing facilities designed for watertightness, often through the use of thin stainless steel liners. The final goal is to characterize the mechanical load induced by consecutive pressure waves in close range to assess the damage to these immersed structures, focusing on both local deformations related to the overall structural response and the direct effects of the explosions, including the liner perforation. The investigation is conducted by the French Institute for Protection and Nuclear Security (DEND), also conducting experimental research into the aerial blast effects of explosions. The institute is developing scaled-down experiments to study shockwave propagation and interaction with reference shapes, such as parallelepiped and cylindrical. Each test is equipped with pressure sensors and high-speed cameras. The French German Research Institute of Saint-Louis (ISL) interest in underwater explosion lies in the study of the mechanisms ruling the transmission of shockwaves through water contained in stainless steel envelopes. Applications include protection of mobile platforms and infrastructures. Preliminary tests have been conducted in free field (without any obstacle near the explosion) inside a reduced-scale basin filled with water, subjected to shockwaves generated by small underwater high-explosive charges. These tests focused on the visualization of the primary shockwave and its spherical propagation in close range, as well as the behaviour of the gas bubble created by the explosion. This paper explores the dynamics of this gas bubble: shape, size evolution, oscillations and migration. Additionally, the study seeks to improve the knowledge of TNT equivalency in aquatic medium, providing insights into the potential hazards associated with underwater explosions and their impact on critical infrastructure.
Keywords: aquatic blast, high-speed imaging, explosive, underwater.

1 INTRODUCTION

The French Institute for Protection and Nuclear Security (DEND) is investigating the impact of aerial explosions, whether accidental or deliberate, on critical infrastructure and transportation systems, with the aim of safeguarding the nuclear industry. To support this objective, scaled experiments are being developed to study the propagation of air blasts and their interaction with target shapes, such as rectangular or cylindrical objects. Diagnostic tools, including pressure sensors and high-speed cameras, are used to collect data.

Since 2017, IRSN has been collaborating with the French German Research Institute of Saint-Louis (ISL) to establish guidelines for conducting reduced-scale explosive tests. In December 2022, the two institutes jointly filed a patent for a novel imaging system. This technology has also been applied to the study of underwater explosive events. Preliminary experiments were carried out at the ISL Explosive Test Range, where glass tanks filled with water were subjected to the pressure effects of a small high-explosive charge placed at the centre.

WIT Transactions on The Built Environment, Vol 215, © 2025 WIT Press
www.witpress.com, ISSN 1743-3509 (on-line)
doi:10.2495/SUSI250041

This paper focuses on capturing the primary shock wave produced by a small-scale underwater explosion and its interaction with a nearby cylindrical object. The goal of these experiments was to determine the feasibility of visualizing and measuring the detailed structure of underwater shock waves as they interact with a convex surface, particularly focusing on incident, reflected, and Mach waves. Objectives also include shockwave propagation investigation, development of small-scale testing protocols in a specifically designed basin, with future work planned in the form of a long-term research project. This involves characterizing wave propagation and the interaction of shock waves with the basin walls and understanding their impact on surrounding structures. Another key goal is to compare the effects of explosions at different depths and positions within the basin, evaluating the differences between seabed and water column detonations. Additionally, the study aims to characterize the TNT equivalency of these explosive charges, determining their explosive potential and evaluating their specific impact in terms of energy release.

Ultimately, the collected data will be used to model these risks and develop predicting tools, ensuring effective protection against potential explosive event. These objectives will be useful to improve the understanding of underwater explosion impacts in confined environments (in spent fuel pools for instance) and to enhance security measures for such scenarios.

2 LITERATURE REVIEW

As in the case of an aerial explosion, a condensed explosive underwater detonation is characterized by a large amount of energy release, a rapid emission of hot pressurized gas (burnt products bubble) and the subsequent transmission of a supersonic pressure wave into the surrounding environment [1].

2.1 Explosive shockwave characteristics in underwater explosions

A typical pressure signal recorded at a certain distance is presented in Fig. 1. When the wave arrives at the considered point, the initial ambient pressure PH (for hydrostatic pressure) undergoes a sharp quasi-instantaneous increase (crossing shockwave duration between 10 and 100 μs) until peak overpressure P_{max}. Pressure then exponentially decreases back to its ambient value. We must keep in mind that recorded pressure in water can reach levels significantly higher than in air (until a few tens of kilobars) for the same considered distances and charges. The underwater wavefront is then much more concentrated than in air, with shockwaves propagating approximately four times faster (about 1480 m/s in water compared to 340 m/s in air). Subaquatic shockwave models by Cole [1] and Swisdack [2] are commonly used to predict parameters such as peak pressure and impulse based on charge size and distance. These models are established for spherical TNT charges and imply peak pressure values ranging between 3.4 and 138 MPa (i.e. 34 and 1,380 bar).

Fig. 2 shows the Kinney and Graham [3] chart (in dotted lines), which predicts the maximum overpressures in air as a function of reduced distance for a spherical TNT charge, in addition to threshold overpressure values for pyrotechnic effects defined by French regulation in Legifrance [4]. The Cole chart, shown in solid lines for the same explosive on the same graph, indicates the maximum overpressures in water as a function of reduced distance. A significant difference in pressure levels is evident depending on the propagation medium. The same explosive charge generates overpressure over much greater distances in water compared to air. For instance, a 1 kg TNT charge produces an overpressure of only 10 bar in air at 1 m, while in water at the same distance, the overpressure remains at 524 bar.

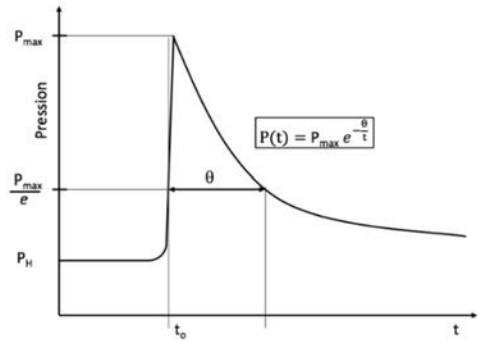

Figure 1: Pressure evolution as a function of time in water medium [1].

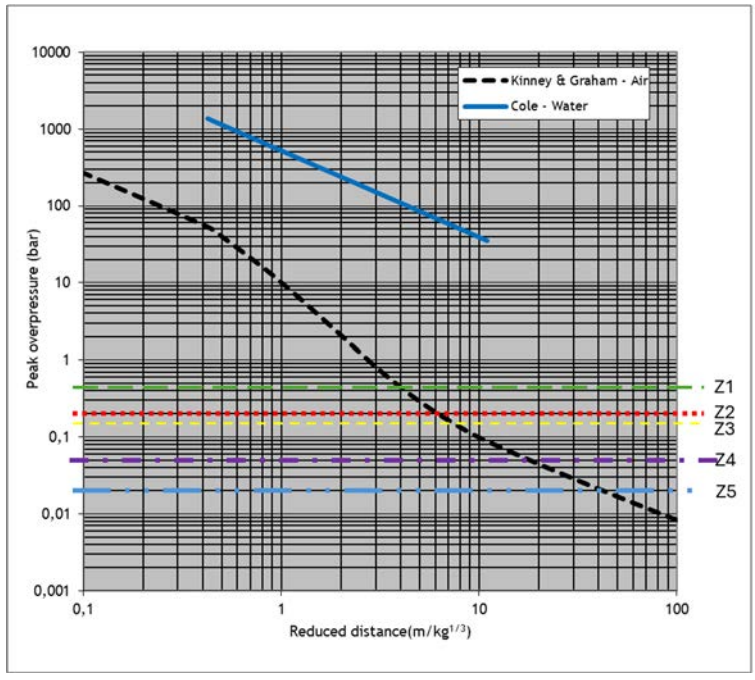

Figure 2: Peak overpressure evolution as a function of reduced distance in water and air medium [1]–[4].

As seen in Fig. 1, the characteristic time θ is defined as the time required for the pressure to fall to a value of $P_{max/e}$. Fig. 3 shows the Cole chart representing this reduced time constant $\theta/W^{1/3}$ where W is the TNT equivalent charge weight in kg, as a function of reduced distance for a spherical TNT charge. A critical parameter to the assessment of underwater blast effects is the distance separating the detonation point from the measuring point location (position of a potential target). Indeed, peak overpressure values rapidly decrease with the distance as shown in Fig. 2. The characteristic time θ also progressively increases with the distance as represented in Fig. 3.

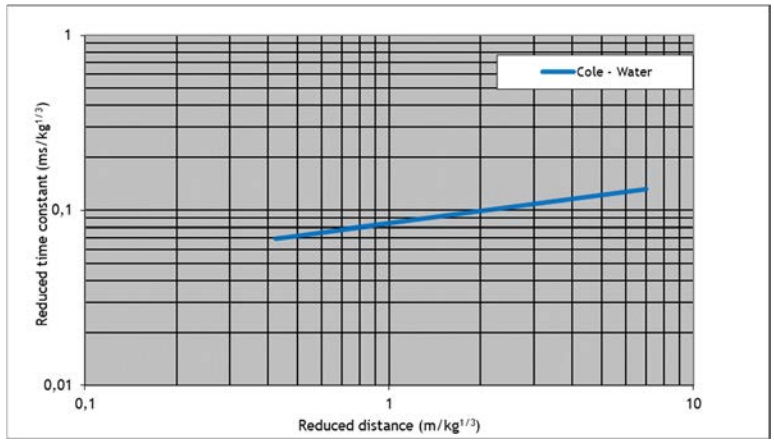

Figure 3: Reduced time constant evolution as a function of reduced distance in water medium [1].

The zones of effects defined in the decree of 2007 [4] setting the rules relating to risk assessment and accident prevention in pyrotechnic establishments and represented as horizontal lines Z_i ($i \in [1;5]$) in the graph of Fig. 2, are specifically designed to assess the risks linked to pyrotechnic activities in the aerial medium. These zones of effects are determined based on various criteria, such as the power and type of pyrotechnic material, to delimit the zones where dangerous effects can occur (for example, detonations, flying debris, bursts, flames, etc.). However, these areas of effect are not supposed to be identical in water. Indeed, the propagation parameters of pyrotechnic effects in an aquatic environment significantly differ from those in the air. Underwater phenomena such as sound propagation, shock waves, and flying debris are influenced by water density, depth, salinity, and other environmental factors (water volume, nature of seabed material, etc.). Therefore, risk assessment and definition of areas of effects underwater must consider these specific differences, such as, for instance, gas bubble dynamics which are qualitatively described in the section hereafter.

2.2 Gas bubble dynamics

After its initial expansion, the burnt products bubble starts to oscillate around the local hydrostatic pressure, while progressively travelling to the surface, as represented in Fig. 4. The end of each new bubble compression transmits a new pressure wave (secondary, then tertiary, etc.) to the ambient medium. This pulsating behaviour is due to the pressure difference between the burnt gases inside the bubble and the surrounding water. The size of the bubble and its initial expansion rate depend on the energy released by the explosion and the depth of detonation.

2.3 Shockwave interaction with target

The mechanical load, consecutive to an underwater explosion, applied to a specific point of an immerged target can be decomposed into three types of waves as illustrated in Fig. 5:

- the incident (or direct) wave that impacts the target with a similar profile as in Fig. 1;

- the compression waves reflected by high impedance surfaces (seabed, subaquatic obstacle, etc.)
- the expansion wave resulting from the reflection on the air interface (low impedance medium).

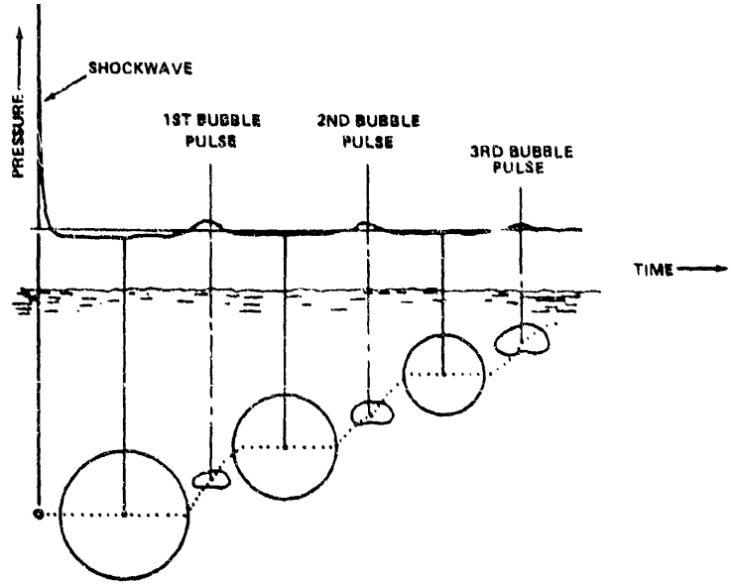

Figure 4: Pressure wave and bubble phenomena of underwater explosion. The upper part shows a pressure–time plot, the lower, the positions and size of the bubble for specific moments which correspond to the curve above as indicated by the vertical lines. *(Source: According to Swisdak [2].)*

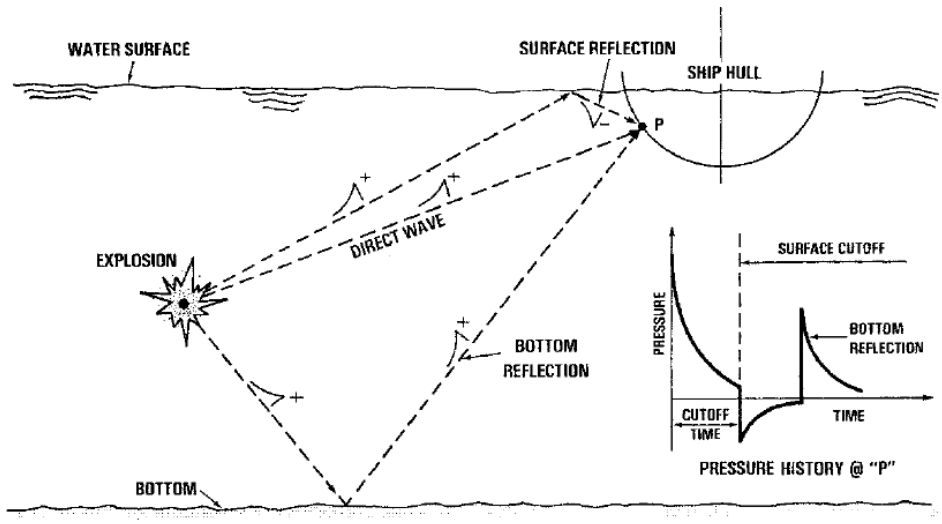

Figure 5: Interaction of underwater explosion waves with a ship hull [5].

In this work, we choose to evaluate underwater explosion effects in free field and close to the tank walls and bed by performing reduced scale experiments.

The experimental studies are conducted in small-scale facilities which allow enhanced monitoring by combining different diagnostic methods and providing the ability to better control and to vary the conditions for shock wave generation and the interaction with various geometrical configurations.

3 EXPERIMENTAL SETUPS

3.1 Underwater blast tanks

A 310.5 litre water steel blasting tank (100 × 60 × 57.5 cm) equipped with polycarbonate windows (presented in Fig. 6) was therefore developed. This set up filled with a mean water height of 54 cm is used to characterize free field overpressures by means of pressure gauge measurements (free field means without any obstacle placed under water, except from tank walls (Fig. 6).

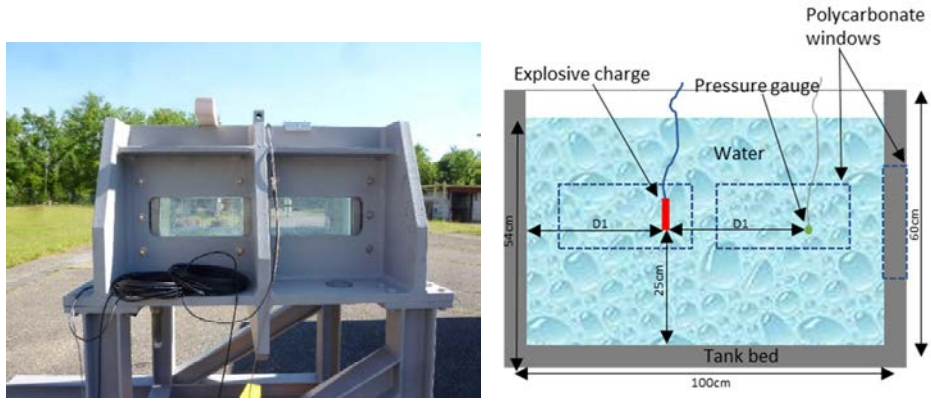

Figure 6: 310.5 litre steel blasting tank.

3.2 Experimental conditions

During the experimental period, a series of 20 underwater explosions using four condensed explosive charges of TNT-equivalent weights ranging from 0.598 g to 10 g (illustrated in Fig. 7) were detonated.

Some experiments were reproduced several times to assess repeatability. The largest charge consists of a plastic explosive bullet (SEMTEX made of RDX and PETN, seen in Fig. 7(d)) stacked together to a bridgewire detonator (namely, a RP501 detonator from Teledyne Defense containing 227 mg of HMX and 136 mg of PETN, see Fig. 7(a)). All the explosive (SEMTEX, RDX, HMX and PETN) weights have been converted into TNT-equivalent weights by applying a TNT-equivalent ratio comprised between 1.45 and 1.72. These ratios, calculated using detonation velocities (according to Cooper methodology [6]), are consistent with the fact that a TNT-equivalent ratio for underwater conditions is higher than for air conditions, as suggested in Cole [1]. However, due to uncertainties on the TNT equivalency for the reduced explosive charges, a ± 10% uncertainty factor is to be considered on the weight of the TNT-equivalent charges.

(a) (b) (c) (d)

Figure 7: Explosive charges. (a) RP83; (b) RP501; (c) RP501 and Semtex (5 g eq. TNT); and (d) RP501 and Semtex (10 g eq. TNT).

The blast wave generated by the detonation of the explosive charge produces a pressure wave measured with piezoelectric sensors in the steel tank. Piezoelectric sensors are PCB M 102A, 102B104 and Neptune Sonar T11 sensors (respectively connected to PCB 482C and 5018 charge amplifiers). Data are recorded and filtered (5th order Bessel filter, 500 kHz) by a 2 MHz Transcom Recorder.

Detonation tests characteristics, including the charge weight, the range distance, the charge depth and the water depth, are presented in Table 1.

Table 1: Characteristics of the explosive tests in steel tank.

Explosive charge	**Weight *W* in TNT eq.[a] (g)**	**Range D_1 (m)**	**Test iterations**	**Water depth (m)**	**Charge depth H (m)**
RP501	0.598	0.35	5	0.54	0.29
RP83	1.89	0.35	3		
RP501 (inversed)	0.598	0.35	1		
RP501	0.598	0.35	5		
RP83	1.89	0.40	1		
RP501	0.598	0.45	2		
RP83	1.89	0.45	1		
RP501 + Semtex	5	0.45	1		
RP501 + Semtex	10	0.60	1		

4 EXPERIMENTAL RESULTS

4.1 Free field results

Fig. 8 presents a comparison of maximal overpressure results from underwater explosions obtained with both sensor technologies (Neptune Sonar, denoted as NS, in Fig. 8(a), and PCB in Fig. 8(b)) with overpressures predicted by Cole (thick line) as a function of the charge weight W (kg) and as a function of the scaled range $D_1/W^{1/3}$ (m/kg$^{1/3}$) where D_1 is the distance from the explosion. Symbols represent experimental data, each point being the mean value

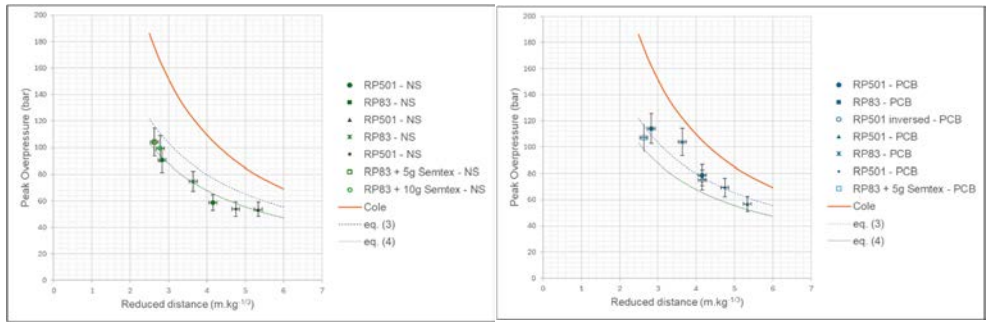

(a) (b)

Figure 8: Variation of the peak overpressure recorded by the various pressure transducers as a function of the scaled range for all explosive charges, detonated in the steel tank.

of a series of tests in the case they have been reproduced. Vertical error bars are based on uncertainties on the maximal peak pressure of ± 10% due to the sensor sensitivity and to the digitizer resolution, and on the standard deviation of the repeated series, which is defined as:

$$\sigma = \sqrt{E[(X - E(X))^2]}, \tag{1}$$

where X represents a series of experimental values.

Horizontal uncertainties on the scaled range are due to the misestimation of ± 10% of the TNT equivalency of the charge as mentioned earlier and to the charge positioning error of ± 0.01 m.

From Fig. 8, it can be observed that the peak pressure decreases with the scaled distance. Moreover, whatever the type of pressure gauge, measurements do not fit the curve for the peak pressure P_{max} (in bar) given by the empirical law (eqn (2)) from Cole reported in the literature (e.g., [1] and [2]) and that applies for shallow charges in deep water:

$$P_{max} = 524\ (D_1/W^{1/3})^{-1.13}, \tag{2}$$

where D_1 is the distance (in m) from the explosion, and W is the charge weight (in kg TNT-equivalent). Instead, for instance, for the PCB gauges, measurements rather follow the curve resulting from the power law fit:

$$P_{max} = 278\ (D_1/W^{1/3})^{-0.9}. \tag{3}$$

For the NS gauges, measurements are well described by the curve resulting from the following law:

$$P_{max} = 233.1\ (D_1/W^{1/3})^{-0.89}. \tag{4}$$

Eqns (3) and (4) significantly differ from eqn (2). In contrast to the empirical law that is defined for an ‘open’ (deep water) environment, eqns (3) and (4) implicitly account for the environment characteristics (essentially, the volume, the small scale and the impedance contrast between water and the tankbed and/or water–air interface). It could be interesting in

the future to see whether the location of the detonation (namely, on the tankbed or close to the water surface) does or not affect the peak pressure.

4.2 Bubble dynamics results

Fig. 9 shows different images of the burnt gas bubble for a RP501 placed at 0.35 m from a PCB sensor in free field, in correlation with recorded pressure–time evolution We observe that, after the detonation, the bubble forms itself and expands (Figs 9(a) and 9(b)) until reaching its maximum radius at 14 ms (Fig. 9(c)); it consequently contracts downwards (Figs 9(d) and 9(e)) before collapsing (Fig. 9(f)).

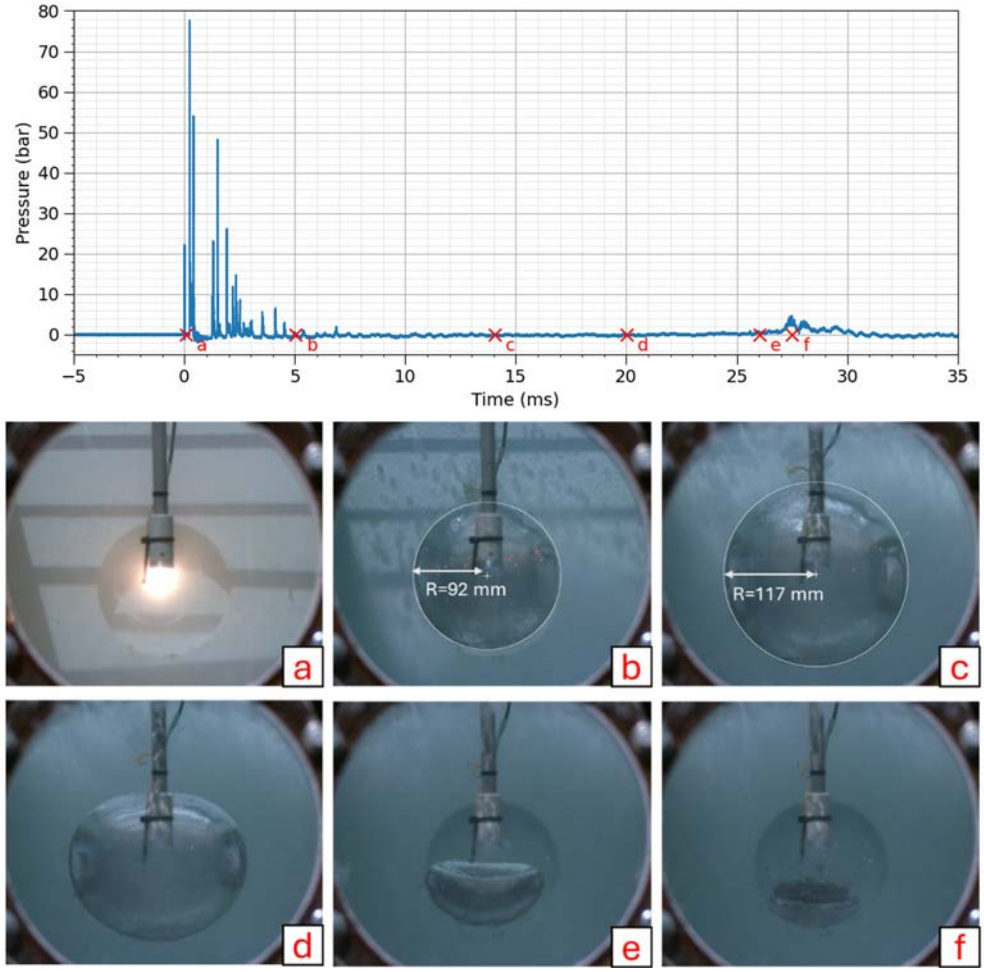

Figure 9: Burnt gas bubble characteristic times and bubble radius *R* evolution (in mm).

At 27.5 ms (Fig. 9(f)), the sensor records an overpressure of approximately 4.5 bar, whereas no significant pressure peak is detected at Figs 9(c), 9(d) and 9(e). This suggests that

the overpressure measured at instant f corresponds to the shock wave generated by the bubble collapse.

The empirical law (eqn (5)) from Cole estimates the first pseudo-period T_p (in ms) (as a function of W, the explosive weight in kg, and H, the explosion depth in m) of the bubble (first reaching a minimum size of the bubble) to be 25.5 ms, which aligns quite well with our recordings of the pressure–time signal and the high-speed videos reported in Fig. 9.

$$T_p = 2.11\ (W^{1/3}/(H+10)^{5/6}). \tag{5}$$

To measure the evolution of the bubble radius over time, the images are post-processed to enhance bubble edges using the MorphoLibJ library [12], followed by a circular Hough Transform analysis in Fiji [13]. This approach provides useful data to describe the bubble during most of its expansion phase, except at the very beginning due to processing issues (as the bubble is quite dark, and when cavitation clouds the window). However, it does not convey the potential asymmetry of the bubble and becomes totally irrelevant during the contraction phase, as the bubble shape transitions from circular to a more jellyfish-like form. To assess the distortion of the bubble, some additional manual measurements of horizontal and vertical radius of the bubble, respectively R_x and R_y in Fig.10, were done. It showcases that even during the expansion phase the bubble tends to grow longer than larger which could be due to interactions with tank walls. The maximum radius R_{max} for this test is estimated to be 117 mm (seen in Fig. 9) which fits well Cole empirical law (136 mm from (eqn (6)) within a 14% difference and considering an approximate uncertainty of 20%.

$$R_{max} = 3.5\ (W/H+10)^{1/3}. \tag{6}$$

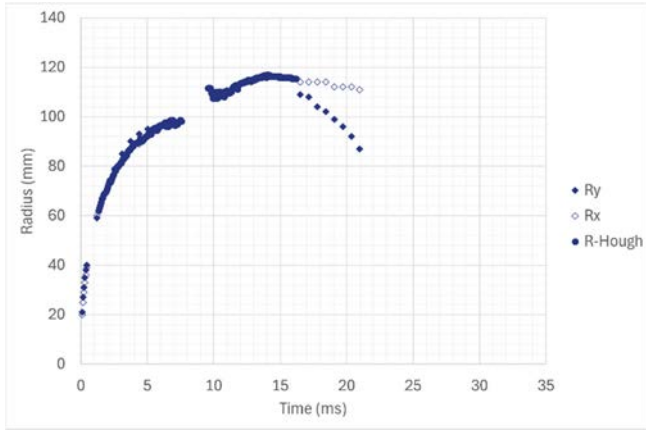

Figure 10: Burnt gas bubble radius over time.

5 CONCLUSION

The study conducted by DEND highlights the importance of understanding the effects of underwater explosions on critical infrastructure. Through reduced-scale experiments, the research focuses on capturing and analysing shockwave dynamics generated by small-scale underwater detonations and their interaction with obstacles. The results reveal valuable insights into the propagation of underwater shockwaves and the behaviour of the burnt gas volume as it collapses on itself. The data collected from pressure measurements and high-

speed imaging has provided a clearer understanding of shockwave characteristics, such as peak pressure and wave propagation (Fig. 10), as well as the impact of detonation distance and charge weight. The findings underscore the significance of environmental factors, such as the volume of the testing area and impedance contrast, which influence the shockwave's behaviour compared to open-water conditions. Moreover, evolution of detonation gas bubble has been observed in detail [11], offering insights into the dynamic response of submerged structures. These experiments form the foundation for developing predictive models and enhancing the design of infrastructure to withstand underwater blast impacts. The next phase of the project will involve testing additional diagnostic methods and comparing experimental results with numerical simulations to further refine these models. This work will contribute to improving safety measures for nuclear infrastructure (such as spent fuel pools notably) exposed to underwater explosive threats.

REFERENCES

[1] Cole, R.H., *Underwater Explosions*, 1st ed., Princeton University Press, 1948.

[2] Swisdak, M., Explosion effects and properties. Part II. Explosion effects in water. Report No. NSWC/WOL/TR-76-116, Defense Technical Information Center, 1978. https://doi.org/10.21236/ada056694.

[3] Kinney, G.F. & Graham, K.J., *Explosives Shocks in Air*, 2nd ed., Springer-Verlag: Berlin, 1985.

[4] Legifrance, Arrêté du 20 avril 2007 fixant les règles relatives à l'évaluation des risques et à la prévention des accidents dans les établissements pyrotechniques. Article 11, 2007. https://www.legifrance.gouv.fr/loda/id/LEGISCTA000006111540.

[5] Costanzo, F.A., Underwater explosion phenomena and shock physics. *Structural Dynamics*, **28**(3), pp. 917–938, 2011.

[6] Cooper, P.W., *Explosives Engineering*, Wiley-VCH: New York, 1996.

[7] Ben-Dor, G., *Shock Wave Reflection Phenomena*, 2nd ed., Springer, 1991.

[8] Gavart, R., Mesure des combinaisons, focalisation et diffraction d'ondes de choc autour de structures type. PhD thesis, University of Orléans, France, 2023.

[9] Kaca, J., An interferometric investigation of the diffraction of a planar shock wave over a semicircular cylinder. Technical Note No. 269, Institute for Aerospace Studies, University of Toronto, 1988.

[10] Zółtak, J. & Drikakis, D., Hybrid upwind methods for the simulation of unsteady shock-wave diffraction over a cylinder. *Computer Methods in Applied Mechanics and Engineering*, **162**(1–4), pp. 165–185, 1998.

[11] Trélat, S. & Sturtzer, M.-O., Blast effects of an underwater explosion: a small-scale approach using high-speed imaging. Presented at *EUROPYRO International Conference*, Saint-Malo, France, 2023.

[12] Legland, D., Arganda-Carreras, I. & Andrey, P., MorphoLibJ: Integrated library and plugins for mathematical morphology with ImageJ. *Bioinformatics*, **32**(22), pp. 3532–3534, 2016. https://doi.org/10.1093/bioinformatics/btw413.

[13] Schindelin, J. et al., Fiji: An open-source platform for biological-image analysis. *Nat. Methods*, **9**, pp. 676–682, 2012. https://doi.org/10.1038/nmeth.2019.